Electronic Supplementary Information

Constructing a Library of Metal and Metal-Oxide Nanoparticle Heterodimers through Colloidal Assembly

Tina A. Gschneidtner,[a] Sarah Lerch, [a] Erik Olsén,[b] Xin Wen,[a] Amelia C. Y. Liu,[c,d] Alicja Stolaś,[a] Joanne Etheridge,[c,e] Eva Olsson,[*,b] Kasper Moth-Poulsen[*,a]

[a] *Department of Chemistry and Chemical Engineering, Chalmers University of Technology, SE-412-96 Göteborg, Sweden*

[b] *Department of Physics, Chalmers University of Technology, SE-412-96 Göteborg, Sweden*

[c] *Monash Centre for Electron Microscopy, Monash University, VIC 3800, Australia*

[d] *School of Physics and Astronomy, Monash University, VIC 3800, Australia*

[e] *Department of Materials Science and Metallurgy, Monash University, VIC 3800, Australia*

Contents Page

S1. Experimental methods

S1.1 *Instruments*

TEM: FEI Tecnai T20 LaB6.
SEM: FEI NovaNano Field Emission Gun SEM fitted with a Delmic SPARC cathodoluminescence system (Andor Shamrock 303i spectrometer with a 150 l/mm grating, Andor iVac spectral camera (2000x256), Andor Zylar 4.2 angle-resolved CMOS detector, Chrma 100 nm bandwidth filters).
Zeta-Potential / **DLS**: Malver Zetasizer Nano ZS.
Centrifuge: Mini Spin, rotor KL125 (9 cm).
Sigma Laboratory Centrifuge 4K15.
Hettich Zentrifugen Universal 32.

S1.2 *Positively charged NPs (NP A)*

All colloidal NP solutions were used without further modification for the dimer formation, according to Table S1.1, below. Their zeta potentials, indicating the charge of the NP surface, and the hydrodynamic radius were measured as described in S1.7, below.

Pd, cubes, CTAB, 25 nm and 80 nm

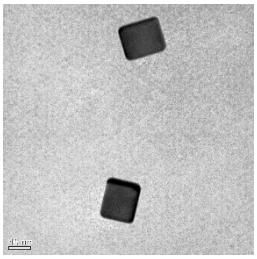

Figure S1-1. Pd cubes, CTAB, 25 nm. Scale bar = 10 nm

The Pd NP were synthesized according to a known procedure,[1,2] in which Pd seeds of the size of 25 nm are prepared and grown to bigger Pd cubes of 80 nm.

The NP solutions need to be optimized in terms of NP concentration and counter ion concentration, in this case, CTAB.

Pd, 25 nm:
The CTAB concentration was reduced to 3 µM (c_1) by centrifugation and the final NP concentration was 8.31 x10^{12} NP/mL.

Pd, 80 nm:
The CTAB concentration was reduced to 3 µM by centrifugation and the final NP concentration was 6.56 x10^{10} NP/mL.

These colloidal NP solutions were used for the dimer formation.

Au, cubes, CTAC, 55 nm

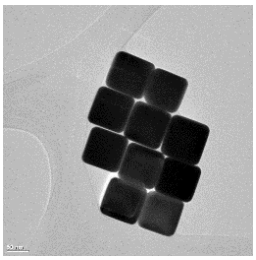

Figure S1-2. Au cubes, CTAC, 55 nm. Scale bar = 50 nm.

The Au cubes were synthesized according to a known procedure,[3] and optimized in order to form heterodimer nanoparticles.

The CTAC concentration was reduced to 5.8 µM (c_1) by centrifugation and the final NP concentration was 1.77 x10^{11} NP/mL.

Au, triangles, CTAB, 63 nm

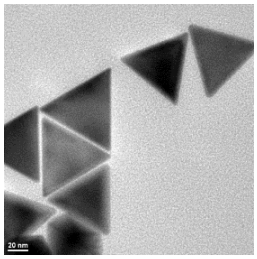

Figure S1-3. Au triangles, CTAB, 63 nm. Scale bar = 20 nm.

The Au triangles were synthesized according to a known procedure,[4] and modified and purified afterwards in order to form heterodimer nanoparticles.

The synthesis does not result in exclusively triangular nanoparticles and requires a purification step. Here, 7 ml of 25% CTAB solution was added to the final reaction mixture, post synthesis, and left overnight to sediment (final CTAB concentration was 0.177 M). The rhombic-shaped by-product remained in solution, while the triangles precipitate.
The precipitate was dispersed in 5 mL, 0.1 M CTAB solution, with an estimated NP concentration of 1.75 mM.

The CTAB concentration was reduced to c_1=50 µM or c_2=5 µM by centrifugation and the final NP concentration was 2.11 x10^{23} NP/mL.

Au, rods, CTAB, 120 nm

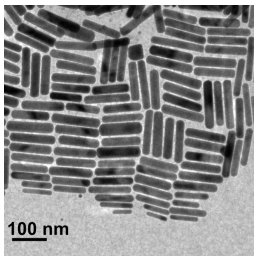

Figure S1-4. Au rods, CTAB, 120 nm. Scale bar = 100 nm.

The Au rods were synthesized according to a known procedure,[5] and modified afterwards in order to form heterodimer nanoparticles.

The CTAB concentration was reduced to 30 µM (c_1) by centrifugation, and to a final NP concentration of 4.1 x10^{22} NP/mL.

Fe_2O_3, cubes, CTAB, 25 nm

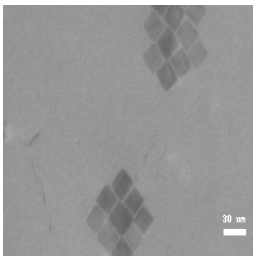

Figure S1-5. Fe_2O_3 cubes, CTAB, 25 nm. Scale bar = 30 nm.

The iron cubes were synthesized according to a known procedure,[6,7] starting to form an iron-oleate complex, which is further used to synthesize monodisperse cubic nanoparticles at a high reaction temperature. The particles were modified and purified afterwards in order to form heterodimer nanoparticles.

The nanoparticles are originally stabilized in oleic acid / oleylamine and need to have an electrostatic charge introduced in order to allow the usage of them in this approach.

The NPs were purified by repeated precipitation and centrifugation from hexane, by adding isopropanol.

10 mg Fe_2O_3 cubes were dispersed in 4 mL chloroform and stirred with 1 mL isopropanol, containing 10 mg CTAB, for 2 days at RT. The solvent was removed and the particles re-dispersed in water, indicating that the formerly hydrophobic NPs are now hydrophilic, due to an intercalation of the CTAB into the oleic acid/oleylamine stabilizer shell of the NPs.

The CTAB concentration was reduced to c_1=2.1 mM, c_2=0.63 mM and c_3=39 µM by centrifugation, and the final NP concentrations of 3.1 $x10^{14}$ NP/mL in c_1, 9.3 $x10^{13}$ NP/mL in c_2 and 5.8 $x10^{14}$ NP/mL in c_3.

TiO_2, truncated rhombic, CTAB, 22 nm

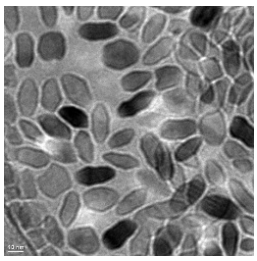

Figure S1-6. TiO_2 truncated rhombic, CTAB, 22 nm. Scale bar = 10 nm.

The TiO2 NPs were synthesized according to a known procedure,[8] and modified afterwards in order to form heterodimer nanoparticles.

The nanoparticles are originally stabilized in oleic acid / oleylamine and need to have an electrostatic charge introduced in order to allow the usage of them in an electrostatic approach.

7 mg TiO_2 NPs were dispersed in 2 ml chloroform, containing 16 mg CTAB, and stirred for 2 days at RT. The solvent was removed and the particles re-dispersed in 4 mL water.

The CTAB concentration was reduced to c_1=5 mM by adding water to the reaction mixture. The final NP concentration of 2 $x10^{17}$ NP/mL is estimated.

S1.3 *Negatively charged NPs (NP B)*

Au, spheres, MesNa/citrate, 30, 60 and 95 nm

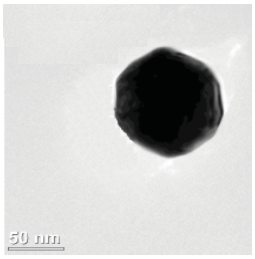

Figure S1-7. Au spheres, MesNa/citrate, 95 nm. Scale bar = 50 nm.

Citrate stabilized Au NPs are commercially available from Sigma Aldrich. These colloidal solutions were stabilized by adding aliquots of the linker sodium 2-mercaptoethanesulfonate (MesNa) solutions as described below.

The citrate NPs were further stabilized with a negatively charged stabilizer, via a sulfur anchor, MesNa. Therefore, 1 mL particle solution (c_{NP}≈3.80 x10^{9} NP/mL, 95 nm NP) was mixed with 50 µL of the linker MesNa solution (6 x10^{-4} M). The solution was incubated overnight on a rocking table and the excess of linker was removed by centrifugation (3000 rpm, 10 min).

The citrate concentration was reduced to c_1=15 µM or to c_2=7.55 µM and by centrifugation, and to a final NP concentration of 1.8 x10^{10} NP/mL for the 30 nm NPs, 1.9x10^{9} NP/ml for the 60 nm NPs and 3.8 x10^{8} NP/mL for the 95 nm NPs.

Pd, cubes, PVP, 7.5 nm

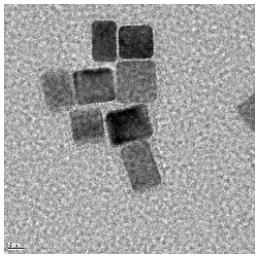

Figure S1-8. Pd cubes, PVP, 7.5 nm

The Pd cubes were synthesized according to a known procedure,[9] and modified afterwards in order to form heterodimer nanoparticles.

The Pd cubes were purified by centrifugation. Therefore, 0.5 mL NP solution was mixed with 0.5 mL ethanol for 120 min at 12000 rpm. This procedure was repeated twice and the final product re-dispersed in 1 mL water.

The PVP concentration was reduced by centrifugation to c_1=1.6 x10^{-11} M, c_2=1.6 x10^{-12} M, c_3= 7.8 x10^{-13} M, c_4= 7.8 x10^{-14} M PVP, or c_5= 1.6 x10^{-14} M, which is, in all cases, negligible. With the centrifugation and dilution series, final NP concentrations for c_1= 1.8 x10^{10} NP/mL, c_2=1.8 x10^{9} NP/mL, c_3=9.23x10^{8} NP/mL, c_4=9.23x10^{7} NP/mL and c_5=1.8x10^{7} NP/mL were achieved and used for the dimer formation.

Au, stars, PVP, 40 nm

PVP stabilized Au nanostars are commercially available from Dianova and used in the concentration (c_1) they were purchased, without purification.

S1.4 *Assembly of heterodimers*

NP A and NP B were mixed according to the table below. The solutions were used immediately after mixing for the preparation of samples for TEM and SEM characterization.

NP A			NP B		
	conc.	vol.		conc.	vol.
Au cubes, 55 nm	c_1	30 µl	Au spheres, 95 nm	c_1	10 µl
Pd cubes, 25 nm	c_1	5 µl	Au spheres, 95 nm	c_1	10 µl
Pd cubes, 80 nm	c_1	5 µl	Au spheres, 95 nm	c_1	10 µl
Au triangles, 63 nm	c_2	10 µl	Au spheres, 60 nm	c_2	5 µl
Au triangles, 63 nm	c_2	10 µl	Au spheres, 95 nm	c_1	5 µl
Fe_2O_3 cubes, 25 nm	c_2	10 µl	Au spheres, 60 nm	c_2	5 µl
Au rods, 120 nm	c_1	20 µl	Au spheres, 30 nm	c_2	20 µl
Au rods, 120 nm	c_1	5 µl	Pd cubes, 7.5 nm	c_5	20 µl
Au triangles, 63 nm	c_1 or c_2	50 µl	Pd cubes, 7.5 nm	c_4 or c_5	10 µl
Au rods, 120 nm	c_1	5 µl	Au stars, 40 nm	c_1	5 µl
Au triangles, 63 nm	c_1	5 µl	Au stars, 40 nm	c_1	5 µl
TiO_2 truncated rhombic, 22 nm	c_1	10 µl	Au spheres, 30 nm	c_2	5 µl
Au triangles, 63 nm	c_2	5 µ	Au spheres, 30 nm	c_1	5 µ
Au rods, 120 nm	c_1	5 µl	Au spheres, 60 nm	c_2	5 µl

Table S1-1. Nanoparticles for heterodimer assembly. NPs on the left (NP A), are positively charged, with CTAB or CTAC, and NPs on the right (NP B) are negatively charged, with MesNa/citrate or PVP. Concentrations (conc.) are referenced in the NP synthesis section (S1.3, S1.4) above and volumes added (vol.) are included in this table.

S1.5 *DLS / zeta-potential: sample preparation & measurements*

For DLS and zeta-potential measurements, the samples were prepared following the procedures described above for the self-assembly experiments. The final volume was adjusted to achieve the minimum volume of solution required for the DLS and zeta-potential cells (0.8 mL), keeping the concentrations of salt and stabilizer constant. In every measurement, the optimal instrument settings lead to reliable data, with good data-quality indicators.

S2. Zeta-potential measurements

S2.1 *Zeta-Potential of positively charged Au NPs (▲, 63 nm) as a function of CTAB concentration*

As one example, Au triangles (63 nm) have as CTAB concentration of 0.1M after synthesis and the zeta-potential for these NPs is +64.7 mV. The amount of CTAB was steadily reduced through repeated centrifuge-washing, and the zeta potential of the particles decreases, indicating a less stable colloidal solution. A value of around +24 mV is measured when the CTAB concentration is reduced to 5 µM, as used for the heterodimeric assembly procedure. This value indicates that the Au triangles are still in a stable colloidal solution.

The zeta-potential measurements were performed at 35 °C with a thermal equilibration time of 2 min. The data shown below are the average of three independent measurements.

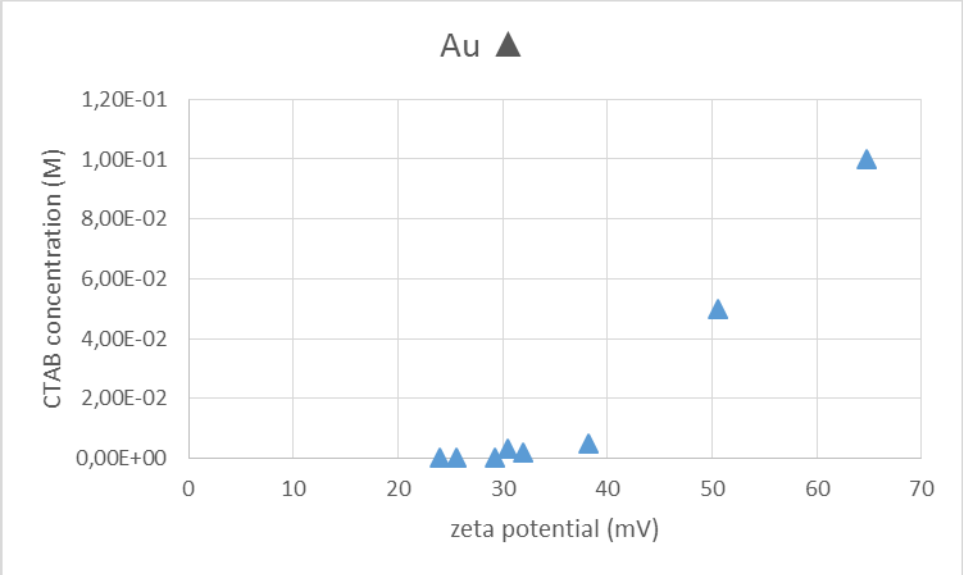

Figure S2.1 Change in zeta-potential for Au triangles (63 nm) as a function of CTAB concentration. CTAB is removed through repeated centrifugal washing steps. Initial synthesis results in 0.1M CTAB concentration, while 5μM corresponds to the concentration used for heterodimer assembly.

S2.2 *Zeta-potential of initially positively charged Au NPs (▲, 63 nm) as a function of the citrate concentration*

While forming dimeric nanoparticles, a certain amount of citrate is added to the CTAB-stabilized solution, e.g. when forming dimers with 30 nm spherical Au NPs. Starting from a zeta potential of +64.7 mV and adding citrate to a final concentration of around 6 µM, the triangle particle solution remains stabilized with a zeta-potential of +22 mV.

Eventually, when too much citrate is added, the triangular particles aggregate and a zeta-potential around +10.0 mV is measured.

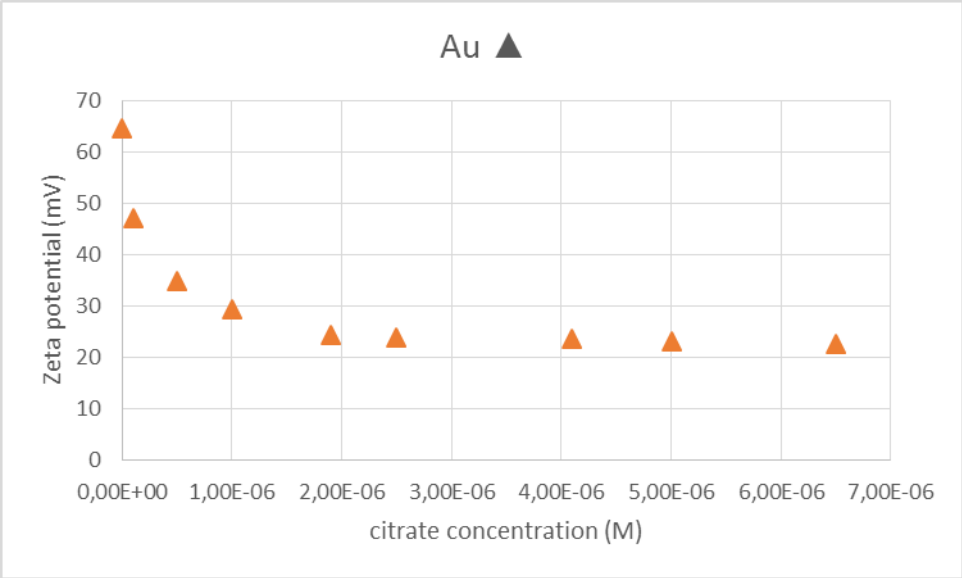

Figure S2.2 Change in zeta-potential for Au triangles (63 nm) as a function of added citrate concentration. Approximately 6μM of citrate corresponds to the expected amount of citrate added during heterodimer assembly.

S2.3 *Zeta-potential of negatively charged Au NPs (●, 30 nm) as a function of citrate concentration*

As an example of a negatively charged particle, Au spheres (30 nm) begin with a citrate concentration of approximately 30 µM (reported by Sigma Aldrich), and the zeta-potential for these particles is -50.6 mV. The amount of citrate was steadily reduced through centrifugal washing, and the zeta potential of the particle increases towards 0 mV, meaning a less stable colloidal solution. A value of around -19 mV is measured, when the citrate concentration is reduced to 7.5 µM, as used for heterodimer assembly. This value indicates that the Au spheres are still in a stable colloidal solution.

The measurements were performed at 35 °C with a thermal equilibration time of 2 min. The shown data are the average of three independent measurements.

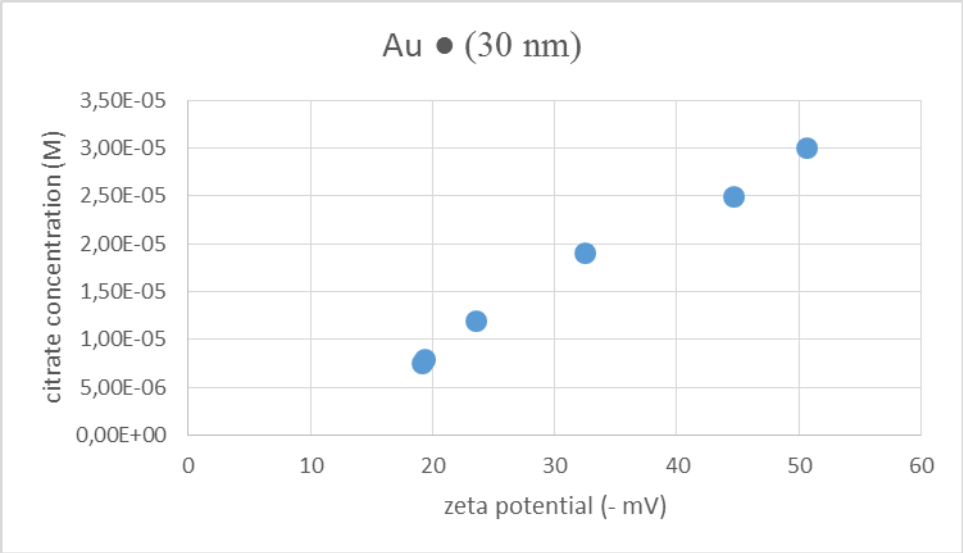

Figure S2.3 Change in zeta-potential for Au spheres (30 nm) as a function of citrate concentration. Approximately 30μM of citrate corresponds to the initial amount of citrate in the colloidal solution, while 7.5μM corresponds to the concentration used for heterodimer assembly.

S2.4 *Zeta-potential of initially negatively charged Au NPs (●, 30 nm) as a function of added CTAB concentration*

The zeta-potential of the spherical, citrate-stabilized Au NPs was observed during the addition of CTAB to the solution. The NP solution started with a zeta-potential of -51 mV, when stabilized in a 30 µM citrate solution. The zeta potential decreases to -5.1 mV when a concentration of 2.8 µM CTAB was achieved, approximately equivalent to the concentration used for heterodimer assembly. The particles were stable for a short time but aggregated soon afterwards.

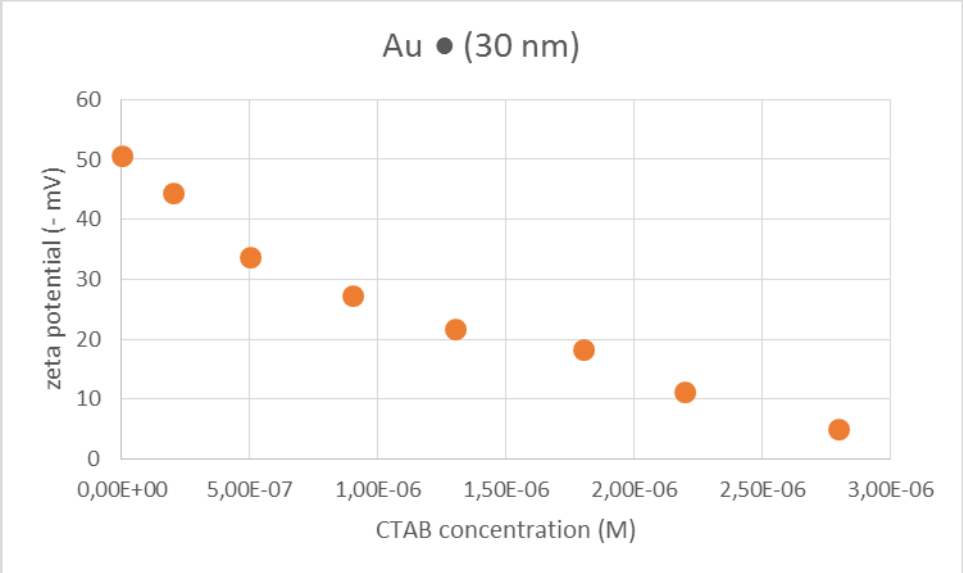

Figure S2.4 Change in zeta-potential for Au spheres (30 nm) as a function of added CTAB concentration. At approximately 2.8μM, which corresponds to the concentration used for heterodimer assembly, the particles are stable for a short time.

S3. Hydrodynamic radius (dynamic light scattering, DLS) / Z-average / zeta-potential of all NPs

The hydrodynamic diameter and the zeta-potential of all nanoparticles were measured using a Zetasizer Nano ZS90 LDS system from Malvern Instruments Ltd., England.

The DLS and zeta-potential measurements were done under the experimental conditions for the dimer formation. We report the Z-average size for the positively charged NPs (NP A), the hydrodynamic radius for the negatively charged NPs (NP B) due to their mainly spherical nature, and the polydispersity index (PDI) for these size measurements, as well as the zeta-potential for all NPs.

NP A	Z-average (nm)	PDI	ζ (mV)
Pd cube, 25 nm	28	< 0.09	20.4
Pd cube, 80 nm	87	< 0.07	20.1
Au triangle, 63 nm	70	< 0.14	23.2
Au rod, 120 nm	21/126	< 0.21	28.5
Fe cube, 25 nm	29	< 0.17	34.4
Au cube, 55 nm	60	< 0.04	29.2
TiO_2 truncated rhombic,	40	< 0.25	38.6

Table S3.1 Size and surface charge measurements for positively charged NPs. Size is reported as the Z-average value, with corresponding polydispersity indices (PDI) and zeta-potentials for each NP solution.

The measurement of the Au rod showed two peaks in the intensity distribution, one for the length, one for the diameter of the rod.

NP B	<r> (nm)	PDI	ζ (mV)
Au sphere, 95 nm	111	< 0.04	-18.1
Au sphere, 60 nm	67	< 0.13	-16.7
Au sphere, 30 nm	34	< 0.2	-19.0
Au star, 40 nm	25	< 0.17	-24.3
Pd cube, 7.5 nm	10	< 0.09	-20.1

Table S3.2 Size and surface charge measurements for negatively charged NPs. Size is reported as the hydrodynamic radii, with corresponding polydispersity indices (PDI) and zeta-potentials for each NP solution.

The zeta potential of all particles is in a regime which is common for stable colloidal NPs.

S4. Typical heterodimers: dimers, clusters and overview TEM images

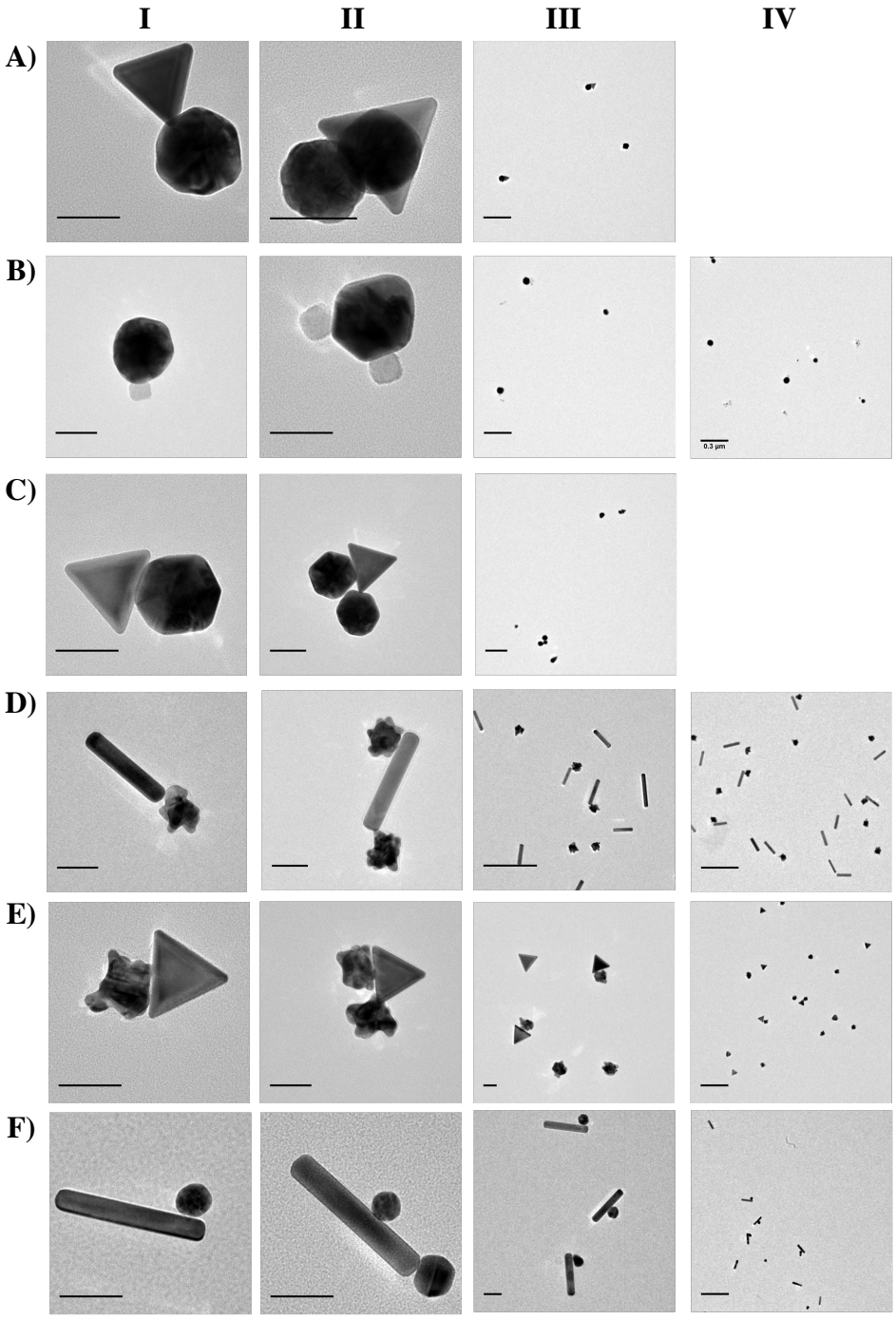

Figure S4.1 TEM images of various heterodimers, indicating dimer formation (I, scale bar = 50 nm), cluster formation (II, scale bar = 50 nm), and overview images to show distribution (III-IV, scale bar = 0.3 μm). **A)** Au triangle, 63 nm and Au sphere, 95 nm. **B)** Fe_2O_3 cube, 25 nm and Au sphere, 95 nm. **C)** Au triangle, 63 nm and Au sphere, 60 nm. **D)** Au rod, 120 nm and Au star, 40 nm. **E)** Au triangle, 63 nm and Au star, 40 nm.

S5. Population statistics for all nanoparticle combinations

Concentrations of NPs, as well as the salt concentrations of citrate and CTAB, are according to the syntheses described in sections S1.3 and S1.4.

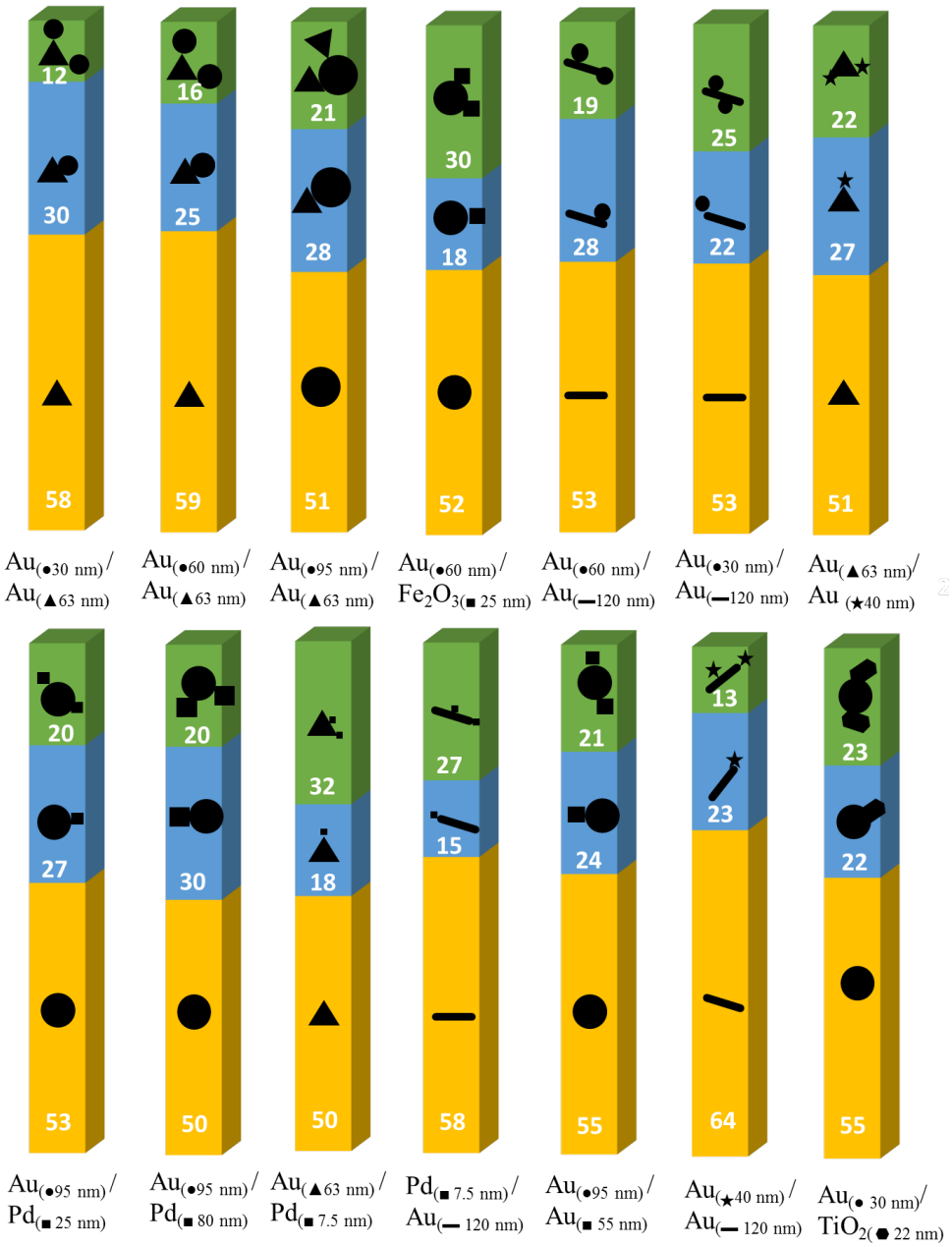

Figure S5.1 Population statistics for each heterodimer assembly as outlined in Table S1.1. Yellow indicates single particles, blue indicates dimers and green indicates larger clusters.

Heterodimer geometries were identified based on the alignment of the corners (or short edges in nanorods) due to the interest in aligned corners to create the strongest hotspots. Yields of these aligned dimers are reported below but there is no indication of a significant alignment in any of the dimers.

	Particle A				Particle B				Total
	NP	shape	size (nm)	Yield of Corners /Short Edges (%)	NP	shape	size (nm)	Yield of Corners /Short Edges (%)	Both Corners (%)
1	Au	triangle	63	17	Au	sphere	30	---	17
2	Au	rod	120	11	Au	sphere	30	---	11
3	TiO_2	rhombic	22	0	Au	sphere	30	---	0
4	Au	triangle	63	13	Au	sphere	60	---	13
5	Fe_2O_3	cube	25	0	Au	sphere	60	---	0
6	Au	rod	120	50	Au	sphere	60	---	50
7	Au	triangle	63	20	Au	sphere	95	---	20
8	Pd	cube	25	40	Au	sphere	95	---	40
9	Pd	cube	80	0	Au	sphere	95	---	0
10	Au	cube	55	14	Au	sphere	95	---	14
11	Au	rod	120	25	Pd	cube	7.5	12.5	0
12	Au	triangle	63	22	Pd	cube	7.5	0	0
13	Au	rod	120	52	Au	star	40	62	34
14	Au	triangle	63	17	Au	star	40	42	0

Table S5.1. Overview of geometries for electrostatically assembled heterodimers (210 dimers). Individual NP yields represent the percentage of individual shapes lining up along corners, when present (see Figure S4.1AI for examples) while the total yield represents the percentage of structures where both NPs involved in the dimer align along the corners or shortest edges (see Figure S4.1DI for example). Dimers with spheres cannot have 2 corners involved, so any spheres that align the corner or short edge of the individual particle are counted as both corners lining up.

S6. Cathodoluminescence (CL) measurements for single NPs

S6.1 *Measurement parameters*

The equipment used for the CL measurements was a FEI Nova NanoSEM equipped with a Delmic SPARC CL system. The FEI Nova NanoSEM was operated at 30 keV with an electron beam with a nominal spot size of 5.5 nm in diameter. The Delmic 13.5 mm working distance mirror was used to collect the CL. The alignment of the mirror relative the NPs was checked before each measurement to maintain similar conditions. The measured heterodimers were all aligned perpendicular to the opening of the mirror towards the camera to make sure that the signal from the two ends of the heterodimer was collected in comparable ways.[10]

For the spectral emission measurements, a two-dimensional grid covering the particle system was set up where each pixel in the grid had a side length of 5 nm. In each pixel, the electron beam was stationary for 400 ms and the resulting emission spectrum was measured between 329-969 nm. A 2 nA electron beam was employed for spectral measurements. During the emission measurements, a drift correction for the particle position was performed every 20 seconds. To minimise the electron dose that the NPs were exposed to, when possible, the drift correction was performed using other features, within the field of view, than the investigated NPs. To every measurement, an additional measurement containing only the substrate was performed immediately afterwards. The region of the substrate was selected so that the distance from neighbouring particles was larger than the characteristic size of the NPs, to ensure that the plasmonic contributions could be neglected, but at the same time as close to the investigated NP system as possible to maintain similar substrate conditions. This substrate measurement was then used to subtract the background contribution in the CL emission.

For the AR-CL measurements, a two-dimensional grid covering the particle system was set up where each pixel in the grid had a side length of around 15-20 nm. To get enough signal statistics, the dwell time at each pixel was increased to 10 seconds and the beam current was increased to 8 nA. During the emission measurements, a drift correction for the particle position was performed every 20 seconds. To every measurement, an additional measurement containing only the substrate was performed directly afterwards. The emission directivity within a certain wavelength region was obtained by inserting a broad band (100 nm) Chroma filter.

For every set of measurements, SEM images were taken both before and afterwards. This was done to check if the exposure to the electron beam had caused a visible change to the nanoparticles. If such a change was observed, the measurement was discarded. Additionally, the stability of the particles was checked by collecting CL data sets on the same particles and confirming that their emission properties were stable after the electron beam exposure.

S6.2 *Data handling for the CL emission spectra*

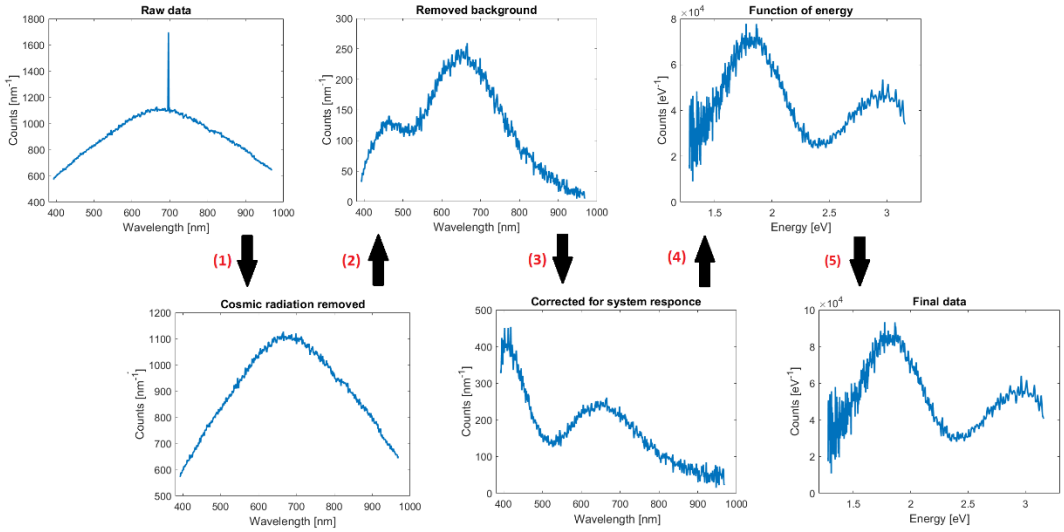

Figure S6.1 Example of the processing steps outlined for the CL data handling.

All data handling was performed using Matlab, where the data processing steps are outlined in Figure S6.1. First, in unprocessed CL data, sharp peaks sometimes appeared at single wavelengths. These peaks originate from cosmic radiation that collide with a detection channel during the measurement. This spurious signal was removed by comparing the signal amplitude with that of the neighbouring values. The method used was to calculate the mean and standard deviation around each electron beam position for every wavelength and if a value deviated more than four standard deviations from the surrounding mean it was replaced by the neighbouring mean value.

After the removal of the contribution from cosmic radiation the background signal was subtracted using a spectral measurement of the near-by substrate. The third step was to compensate for the system response function over the measured wavelength region. To derive the system response function, CL measurements were performed on a flat single crystal aluminium substrate and the result was compared with that from theoretical calculations based on the derived equations in ”Optical excitations in electron microscopy” by F. J. García de Abajo[11] together with dielectric data for aluminium.[12]

The fourth step of the data processing was a transformation of the spectral data from a function of wavelength to a function of energy. The transformation was performed by using a Jacobian transformation which compensates for the uneven sampling in energy space, with the condition that the total integrated signal is the same before and after the transformation.[13]

The fifth step of the data processing compensates for potential variations in electron beam current and alignment of the optical system. The normalisation was performed by introducing the condition that the background signal containing only the near-by substrate should have the same amplitude in all

measurements. Therefore, if the amplitude of the background spectra had changed it was attributed to be due to a change in electron beam current. By choosing a reference value based on typical background amplitudes, all the data was normalised with the ratio between the recorded background amplitude and the reference value.

S6.3 *Angle resolved CL (AR-CL) data*

The processing of the AR-CL emission directivity data was performed using Odemis Viewer from Delmic BC, where the software transforms the captured images to emission directivity plots. The software loads the measurement file and subtracts the signal from the background measurement. The polar plots (azimuth, polar) were then exported to Matlab to control the display parameters.

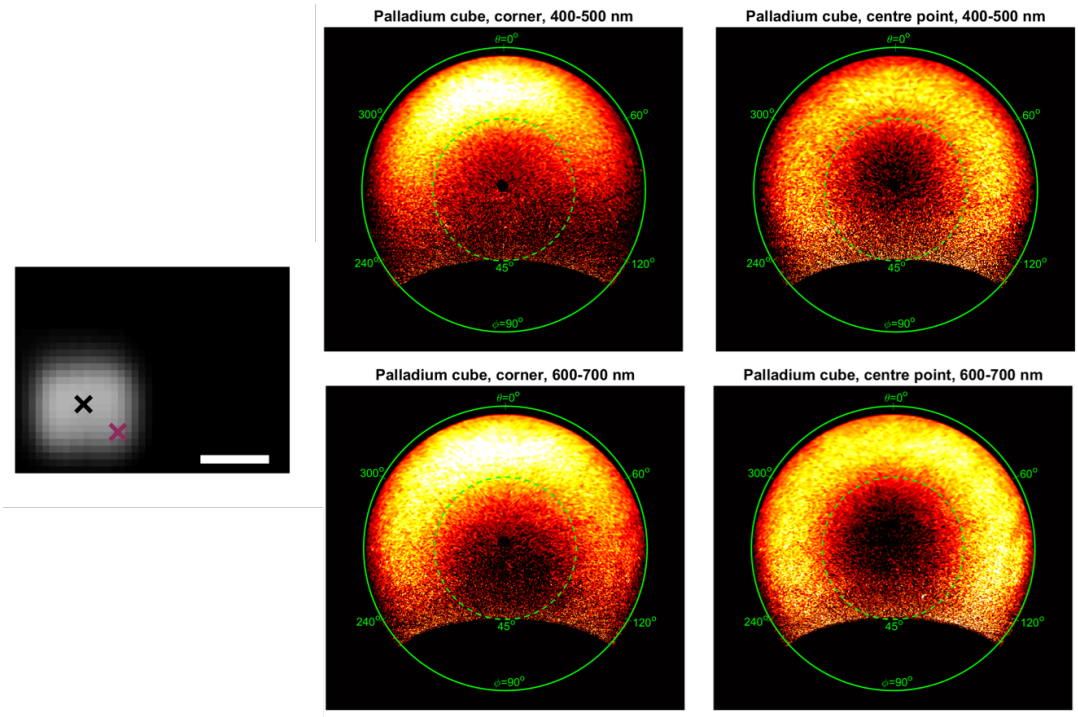

Figure S6.2 AR-CL, from 400-700 nm, for the same palladium cube, 85 nm, as in the main text, Figure 6A, where the measurement points are indicated in the SEM image, shown on the left.

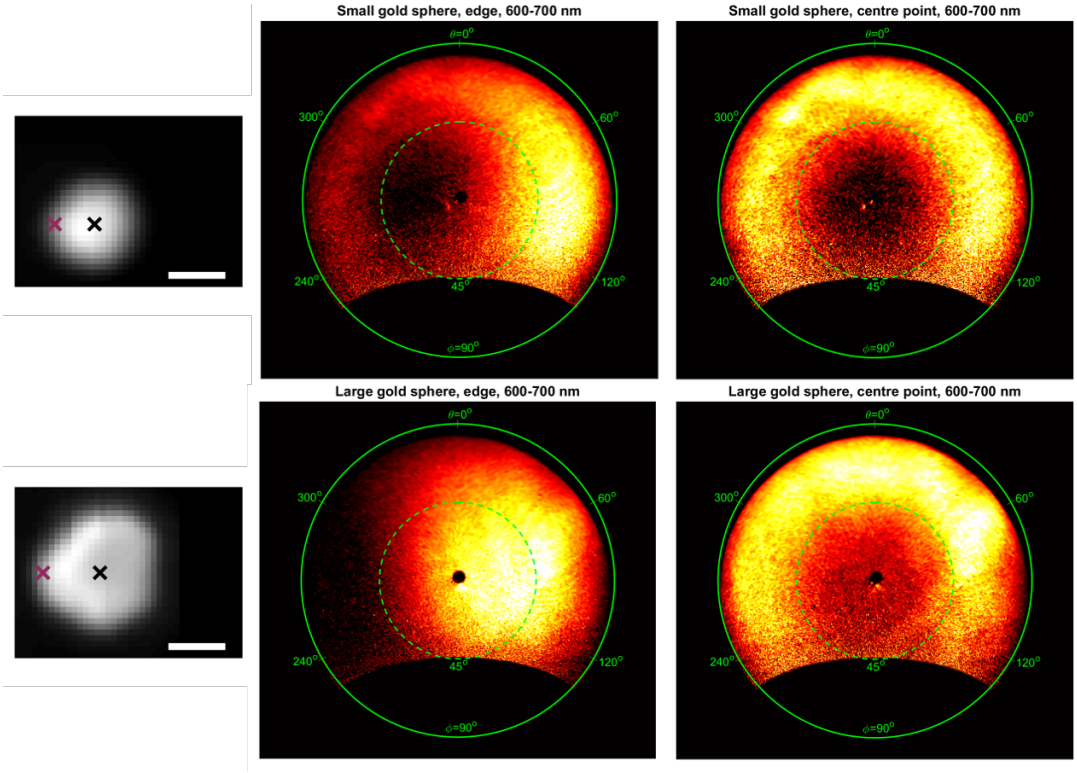

Figure S6.3 AR-CL, for energies from 600-700nm, for the same gold spheres (small, upper = 90 nm; large, lower = 110 nm) as in the main text, Figures 6B-6C, where the measurement points are indicated in the SEM images, shown on the left.

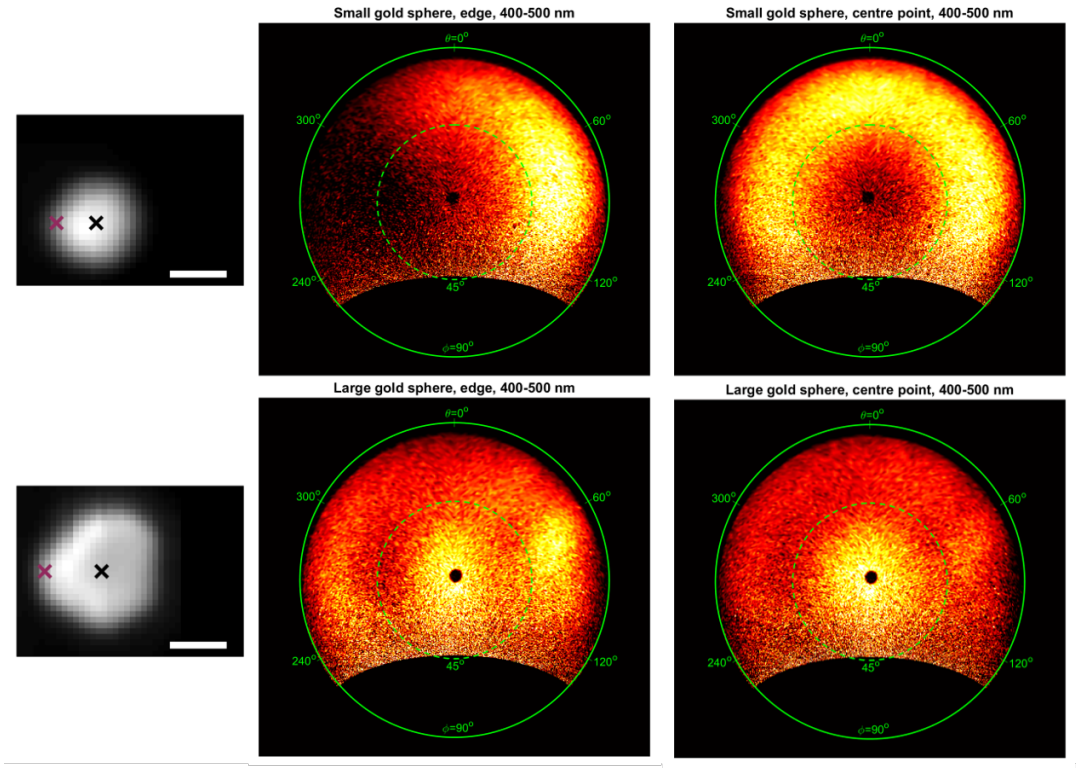

Figure S6.4 AR-CL, for energies from 400-500nm, for the same gold spheres (small, upper = 90 nm; large, lower = 110 nm) as in the main text, Figures 6B-6C, where the measurement points are indicated in the SEM images, shown on the left.

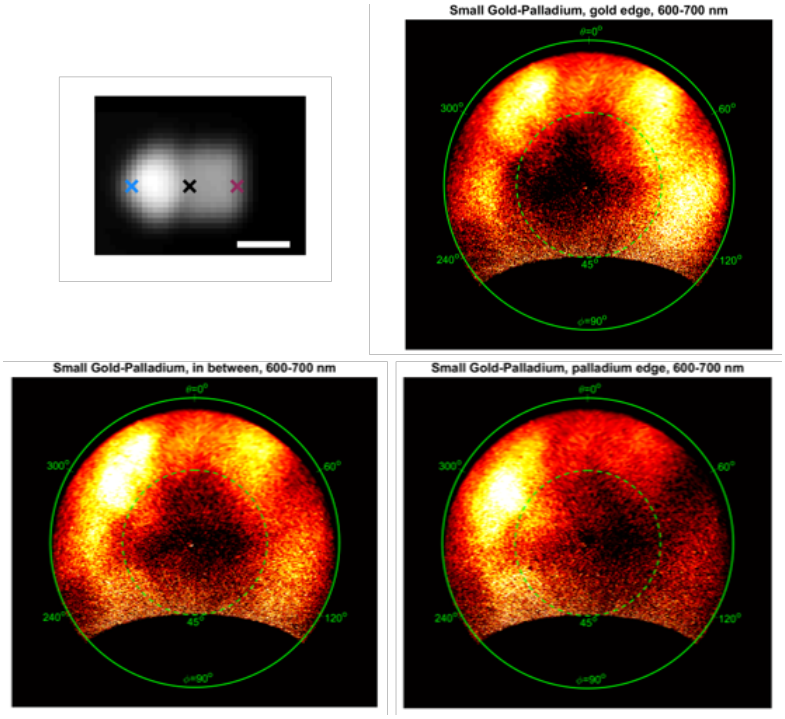

Figure S6.5 AR-CL for the same small gold-palladium heterodimer as in the main text, Figure 6D, where the measurement points are indicated in the SEM images, shown on the top left (gold, on left = 90 nm; palladium, on right = 85 nm).

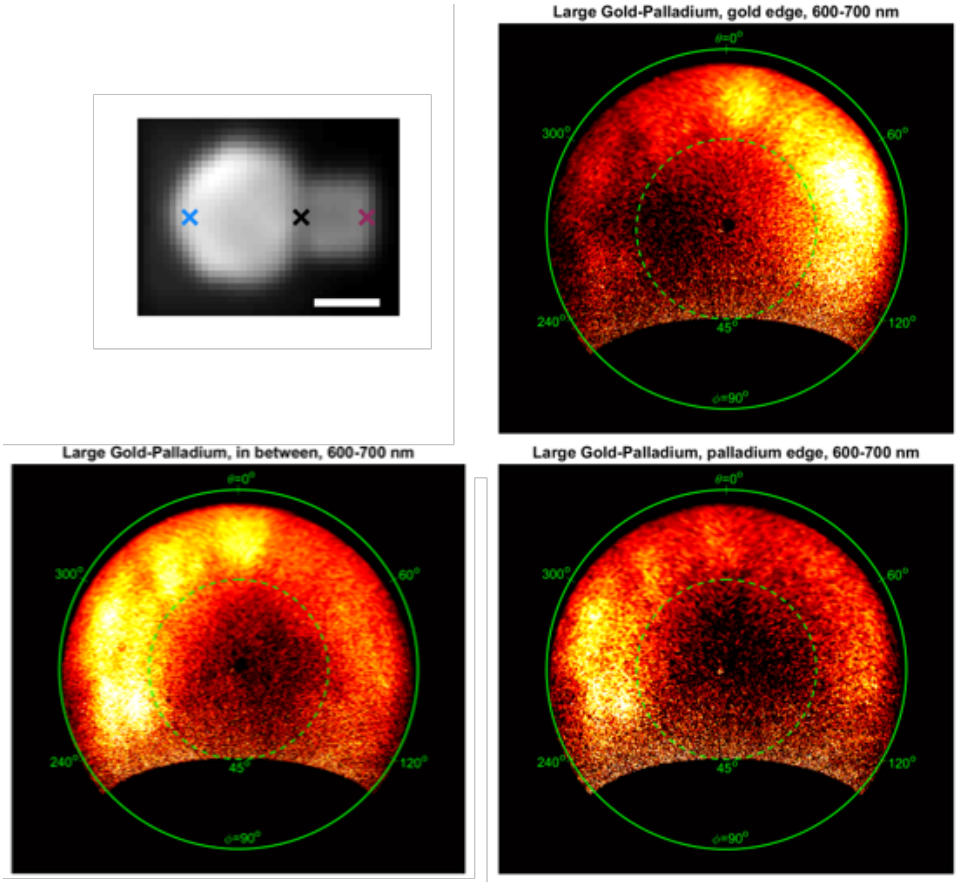

Figure S6.6 AR-CL for the same large gold-palladium heterodimer as in the main text, Figure 6E, where the measurement points are indicated in the SEM images, shown on the top left (gold, on left = 110 nm; palladium, on right = 85 nm).

References

1 W. Niu, Z.-Y. Li, L. Shi, X. Liu, H. Li, S. Han, J. Chen and G. Xu, *Cryst. Growth Des.*, 2008, **8**, 4440–4444.

2 W. Niu, L. Zhang and G. Xu, *ACS Nano*, 2010, **4**, 1987–1996.

3 H.-L. Wu, C.-H. Kuo and M. H. Huang, *Langmuir*, 2010, **26**, 12307–13.

4 L. Scarabelli, M. Coronado-Puchau, J. J. Giner-Casares, J. Langer and L. M. Liz-Marzán, *ACS Nano*, 2014, **8**, 5833–5842.

5 X. Ye, C. Zheng, J. Chen, Y. Gao and C. B. Murray, *Nano Lett.*, 2013, **13**, 765–771.

6 M. Pauly, B. P. Pichon, P.-A. Albouy, S. Fleutot, C. Leuvrey, M. Trassin, J.-L. Gallani and S. Begin-Colin, *J. Mater. Chem.*, 2011, **21**, 16018.

7 N. Pinna, J. F. Hochepied, M. Niederberger and M. Gregg, *Phys. Chem. Chem. Phys.*, 2009, 11, 3607.

8 C. Dinh, T. Nguyen, F. Kleitz and T. Do, *ACS Nano*, 2009, **3**, 3737–3743.

9 B. Lim, H. Kobayashi, T. Yu, J. Wang, M. J. Kim, Z.-Y. Li, M. Rycenga and Y. Xia, *J. Am. Chem. Soc.*, 2010, **132**, 2506–2507.

10 T. Coenen, University of Amsterdam, 2014.

11 F. J. García de Abajo, *Rev. Mod. Phys.*, 2010, **82**, 209–275.

12 E. Palik, *Handbook of Optical Constants of Solids*, Academic Press, 1st edn., 1998.

13 J. Mooney and P. Kambhampati, *J. Phys. Chem. Lett.*, 2013, **4**, 3316–3318.